

Remarkable Ligand Effect in Ni- and Pd-Catalyzed Bisthiolation and Bisselenation of Terminal Alkynes: Solving the Problem of Stereoselective Dialkyldichalcogenide Addition to the C≡C Bond

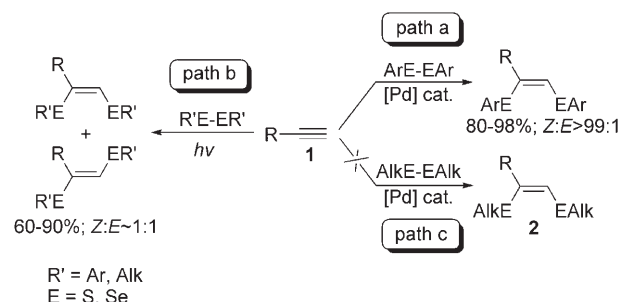
Valentine P. Ananikov,^{*,[a]} Konstantin A. Gayduk,^[a] Irina P. Beletskaya,^{*,[b]} Victor N. Khrustalev,^[c, d] and Mikhail Yu. Antipin^[c, d]

Abstract: We have developed two new catalytic systems based on Ni and Pd complexes to solve the challenging problem of dialkyldichalcogenide (Alk₂E₂; E = S, Se) addition to alkynes. A comparative study of two catalytic systems—Ni/PMe₂Ph and Pd/PCy₂Ph—has revealed that the Ni catalyst is superior with respect to high catalytic activity and more general scope relative to the Pd system. A novel synthetic methodology was developed for the preparation of (*Z*)-bis(alkylthio)alkenes and (*Z*)-bis(alkylseleno)alkenes from terminal alkynes with excellent stereoselectivity and high yields.

Keywords: alkynes • chalcogens • heterogeneous catalysis • nickel • palladium

Introduction

In the pioneering work, A. Ogawa et al.^[1] described the stereoselective addition of Ar₂S₂ and Ar₂Se₂ to terminal alkynes by using a palladium catalyst (path a; Scheme 1).^[2] We have shown that an excess of the phosphane ligand is required to achieve a high yield in this reaction.^[3] By utilizing Pd complexes and an excess of the phosphane ligand, new synthetic protocols have been developed to perform the Ar₂E₂ addition to alkynes in a molten state (solvent free conditions) and with a polymer-supported catalyst.^[4] An un-



Scheme 1. Addition of diaryldichalcogenides and dialkyldichalcogenides to alkynes.

selective non-catalytic side reaction (path b; Scheme 1) was totally suppressed in the case of regular alkynes and the contribution of the side reaction was significantly reduced in the case of activated alkynes.^[3] However, the Pd catalyst showed rather poor efficiency in the case of the dialkyldichalcogenide (Alk₂E₂; E = S, Se) addition to alkynes (path c; Scheme 1), this reaction required a more active Rh catalyst.^[5]

A similar reactivity pattern was observed in another reaction, that is, the transition-metal-catalyzed addition of thiols and selenols (REH; R = Ar, Alk; E = S, Se) to alkynes. This reaction provides a convenient synthetic route to α -substituted vinylchalcogenides with high regioselectivity (Markovnikov-type addition).^[2,3] Pd catalysts were utilized for the addition of arylthiols and arylselenols to alkynes,^[6] however,

[a] Prof. V. P. Ananikov, K. A. Gayduk
Zelinsky Institute of Organic Chemistry
Russian Academy of Sciences, Leninsky Prospect 47
Moscow, 119991 (Russia)
Fax: (+7) 495-135-5328
E-mail: val@ioc.ac.ru

[b] Prof. I. P. Beletskaya
Lomonosov Moscow State University, Chemistry Department
Vorob'evy gory, Moscow, 119899 (Russia)
Fax: (+7) 495-939-3618
E-mail: beletska@org.chem.msu.ru

[c] Dr. V. N. Khrustalev, Prof. M. Yu. Antipin
Nesmeyanov Institute of Organoelement Compounds
Russian Academy of Sciences, Moscow (Russia)

[d] Dr. V. N. Khrustalev, Prof. M. Yu. Antipin
Department of Natural Sciences
New Mexico Highlands University
Las Vegas, NM 87701 (USA)

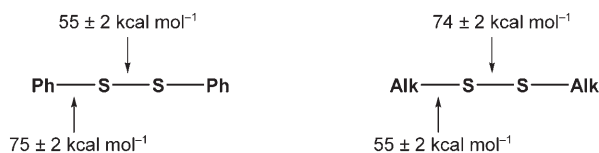
addition of alkane thiols was carried out only with a Rh catalytic system.^[7]

Recently, we have reported on the heterogeneous catalytic system, with $[\text{Ni}(\text{EAR})_2]_n$ as a polymeric catalyst, that lead to the addition of ArEH to alkynes with excellent selectivity and yields under mild conditions (80–99% yields, >95:5 selectivity).^[8] On the other hand, the $[\text{Pd}(\text{EAlk})_2]_n$ polymer was the material of choice for constructing a network of 1D nanobelts, which was a remarkable catalyst for the reaction between alkane thiols and alkynes, resulting in 70–99% yield and >95:5 selectivity.^[9] It was the first successful example of the replacement of Rh complexes by Pd in the catalytic addition reaction involving AlkE groups.

These fascinating results gave us a hope to overcome the problem of Alk_2E_2 addition to alkynes and encouraged us to carry out a comparative study of the catalytic activity of Ni and Pd complexes.

The products of Alk_2E_2 addition to alkynes, (*Z*)-bis(alkylthio)alkenes and (*Z*)-bis(alkylseleno)alkenes (**2**), are in demand in various synthetic transformations and in materials science.^[10,11] Undoubtedly, development of simple and efficient synthetic procedure is required to further explore the potential of such compounds.

To understand the mechanistic nature of the problem, it is worth considering the difference in bond dissociation energies between the diaryldisulfides and dialkyldisulfides. The S–S bond in diphenyldisulfide is considerably weaker than the C–S bond, as reflected by the values of bond dissociation energy (Scheme 2). The opposite relationship is



Scheme 2. C–S and S–S bonds dissociation energy.^[12]

observed in the case dialkyldisulfide: the S–S bond is stronger than the C–S bond by $\approx 20 \text{ kcal mol}^{-1}$. Therefore, a more efficient catalyst should be designed to break the stronger S–S bond of dialkyldisulfides as opposed to the easier case of diaryldisulfides. In addition to high efficiency, the catalyst should be very selective for breaking the strong S–S bond and not to have an effect on the weak C–S bond. The difference between the substrates outlines the principal difficulties in carrying out the desired catalytic transformation (compare paths a and c, Scheme 1). The same considerations are also applicable for the Se analogues and will not be repeated here.

In the present article we describe a novel catalytic system for carrying out the stereoselective addition of dialkyldisulfides and dialkyldiselenides to alkynes in good yields. Cheap and easily available Ni compounds were utilized as catalysts. The key findings concerning the ligand of choice and reliable reaction conditions will be discussed in view of a plausible reaction mechanism. Wherever possible Pd-based cata-

lytic systems were also developed and the scope of both the Ni- and Pd-catalyzed transformations has been investigated in a comparative manner.

Results

Ni-catalyzed bithiolation and bis-selenation of alkynes: The performance of the catalytic system was studied by using dibutyldisulfide addition to 1-hexyne (**1a**) as a model reaction. Initial investigation of the ligand effect was carried out in benzene at 80°C for 4 h. Under these conditions traditional Pd^0/PPh_3 catalytic system catalyzes Ar_2S_2 addition to **1a**, but failed to catalyze Bu_2S_2 addition (only traces of **2a** were detected). Simple replacement of Pd complex by Ni did not improve the catalytic activity of the studied system (entry 1, Table 1). Utilization of various arylphosphanes with elec-

Table 1. Ligand effect on the yield of **2a** in Ni-catalyzed reaction of Bu_2S_2 and 1-hexyne.^[a]

$\text{Bu}-\text{C}\equiv\text{C} + \text{BuS}-\text{SBu} \xrightarrow[\text{benzene, 4h, 80}^\circ\text{C}]{\substack{3 \text{ mol\% } [\text{Ni}(\text{acac})_2] \\ 30 \text{ mol\% L}}} \text{Bu}-\text{C}(\text{SBu})=\text{C}(\text{SBu})$				
Ligand (L)	Yield [%]	Ligand (L)	Yield [%]	
1	0	11	dppe	0
2	0	12	dppb	9
3	0	13	PCy ₃	0
4	0	14	PCy ₂ Ph	0
5	0	15	PCyPh ₂	0
6	0	16	PPh ₂ (CH ₂ Ph)	2
7	0	17	PEtPh ₂	4
8	0	18	PMePh ₂	10
9	7	19	PBu ₃	30
10	3	20	PMe ₂ Ph	38

[a] Bu_2S_2 (1 mmol) and 1-hexyne (1 mmol) in benzene (0.5 mL).

tron-donor and electron-acceptor substituents did not lead to desired product (entry 2–6, Table 1). The first favorable evidence was obtained when using phosphite ligands (entries 9, Table 1). The catalytic system based on the tri(isopropyl)phosphite resulted in 7% of **2a** (entries 9, Table 1), while tributylphosphite and triphenylphosphite were inactive (entries 7, 8, Table 1). A minor increase in the yield up to 9% was obtained with bidentate ligand bis(diphenylphosphino)butane (dppb) (entry 12, Table 1), bis(diphenylphosphino)methane (dppm) gave a trace amount of the product (3%) and bis(diphenylphosphino)ethane (dppe) was totally inactive (entries 10, 11; Table 1). Introducing bulky alkyl group (Cy) into the ligand did not lead to **2a** (entries 13–15, Table 1), but the presence of less bulky alkyl groups in the phosphane ligand increased the yield of **2a** to 10% (entries 16–18, Table 1). Surprisingly, good yield of the product (30%) was observed with PBu_3 ligand (entry 19, Table 1), and even better yield of 38% was found in the case of PMe_2Ph (entry 20, Table 1). Further optimization of the reaction conditions were carried out with the most promising PMe_2Ph ligand. The catalytic reaction with this

ligand was highly stereoselective, with only the formation of the *Z* isomer (*syn* addition) being observed.

Prolonging the reaction time to 8 and 12 h increased the yield of **2a** to 55 and 60%, respectively (entries 1,2; Table 2). Unfortunately, further heating at 80°C did not

Table 2. The yield of **2a** at different temperatures in solvent and under solvent free conditions.^[a]

	Solvent	<i>T</i> [°C]	<i>t</i> [h]	Yield [%]
1	benzene	80	8	55
2	benzene	80	12	60
3	benzene	100	1.5	61
4	benzene	100	2	65
5	benzene	100	2.5	66
6	benzene	100	4	60
7	acetone	100	4	58
8	toluene	100	4	54
9	THF	100	4	52
10	solvent free	70	4	23
11	solvent free	80	4	46
12	solvent free	100	1	57
13	solvent free	100	2	87
14	solvent free	100	4	50
15	solvent free	110	2	67

[a] Bu₂S₂ (1 mmol), 1-hexyne (1 mmol), [Ni(acac)₂] (3 mol%), PMe₂Ph (30 mol%) in solvent (0.5 mL) or solvent free.

improve the yield. Slightly better yields of 61–66% were observed by carrying out the reaction at 100°C (entries 3–5, Table 2). It is very important to point out that longer heating caused a decrease in the yield of **2a** (entry 6, Table 2). Trying different media for the reaction did not solve the problem, leading to <60% yield of the product (entries 7–9, Table 2). Much better results were found by applying a solvent-free reaction under optimized conditions (entries 10–13, Table 2). Carrying out the catalytic reaction at 100°C for 2 h led to 87% of **2a**. At this point (2 h) the alkyne was completely consumed, while some Bu₂S₂ (≈5–10%) remained unreacted. This suggests that the alkyne was involved in a side reaction. Longer reaction time again resulted in a decrease of the yield of **2a** (entry 14, Table 2). The yield of **2a** observed at 110°C (entry 15, Table 2) was smaller than that observed at 100°C (entry 13, Table 2) indicating that further increase of the temperature is not feasible. Therefore, 100°C and 2 h were found to be a good estimate of reliable reaction conditions. The reasons of decreasing product yield at higher temperature or longer time as well as the nature of the side reactions will be analyzed further on.

We have found that the amount of phosphane ligand plays an important role in the studied catalytic system (Table 3). In both cases—reaction in benzene and under solvent-free conditions—the best results were achieved with the ratio Ni:L=1:10 (entry 2, Table 3). Using smaller (entry 1, Table 3) or greater (entries 3, 4; Table 3) ratios diminished the performance of the catalytic reaction.

In all reactions throughout the article 3 mol% of Ni compound was used; an attempt to increase amount of the cata-

Table 3. The yield of **2a** in Ni-catalyzed reaction with different amounts of the PMe₂Ph ligand.^[a]

	Ligand [mol %]	Yield [%]	
		solvent free	in benzene ^[b]
1	15	67	58
2	30	87	65
3	45	78	63
4	60	75	60

[a] Bu₂S₂ (1 mmol), 1-hexyne (1 mmol), [Ni(acac)₂] (3 mol%) and given amount of PMe₂Ph ligand (100°C, 2 h). [b] In benzene (0.5 mL).

lyst did not lead to further improvements, probably due to solubility reasons.

Finally, we studied the influence of the Bu₂S₂:alkyne ratio on the yield of product **2a** (Table 4). Use of an excess of the

Table 4. [Ni(acac)₂]/PMe₂Ph catalyzed reaction with different Bu₂S₂:**1a** ratios.^[a]

	Bu ₂ S ₂ : 1a	Yield ^[b] [%]	
		solvent free	in benzene ^[c]
1	2:1	66	58
2	1:1	87	73
3	1:2	90	80
4	1:3	95	94

[a] Bu₂S₂ (1 mmol), 1-hexyne (1 mmol), [Ni(acac)₂] (3 mol%), and PMe₂Ph (30 mol%) (100°C, 2 h). [b] For entry 1 the yield was calculated based on initial amount of **1a**; for entries 2–4 based on initial amount of Bu₂S₂. [c] In benzene (0.5 mL).

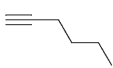
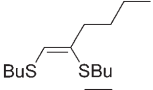
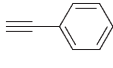
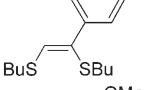
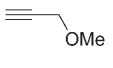
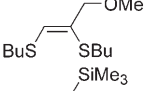
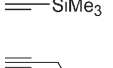
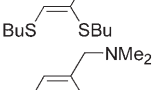
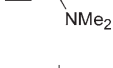
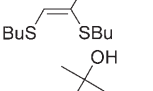
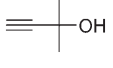
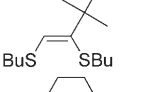
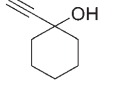
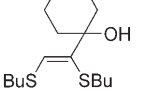
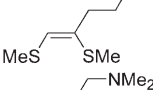
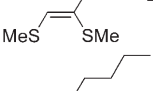
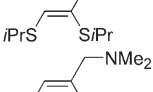
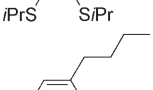
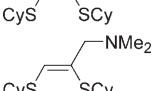
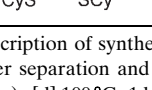
Bu₂S₂ over **1a** decreased the yield of **2a** compared to equimolar ratio of the reagents (entries 1, 2; Table 4). Use of an excess of the alkyne over Bu₂S₂ led to noticeable improvement, reaching a 95% yield at a Bu₂S₂:**1a**=1:3 ratio (entries 3, 4; Table 4).

The scope of the developed catalytic system was investigated for a variety of terminal alkynes^[13] and dialkyldisulfides with different substituents (Table 5). The scope of the catalytic system will be discussed for the substrates ratio Bu₂S₂:alkyne=1:3, which results in better yields. Despite the lower yields, the data on the equimolar Bu₂S₂:alkyne ratio is also presented in Table 5, since this protocol is economic in terms of consumed alkyne and could be also useful in some cases.

Non-activated (**1a**) and activated (**1b**) alkynes reacted with Bu₂S₂ in good yields and selectivity (entries 1, 2; Table 5); this result is an important advantage of the developed catalytic system. For instance, known synthetic procedures of Ar₂S₂ addition to activated alkynes usually result in poor yields and stereoselectivity.^[14]

Our catalytic system was tolerant to functional groups in alkynes leading to high yields and excellent selectivity for **1c–1e** (entries 3–5, Table 5). The only exception was observed for alkynes bearing an OH group (entries 6, 7; Table 5). In these cases we were unable to improve the yield of desired addition product by applying a 1:3 reagent ratio, due to quick polymerization of the alkynes and tar formation. To avoid polymerization in the case of **1f**, the reaction

Table 5. The scope of the Ni-catalyzed addition of dialkyldisulfides to alkynes.^[a]

Alkyne	RS-SR	Product ^[b]	Yield ^[b] [%]	
			R ₂ S ₂ : 1 = 1:1 ^[c]	R ₂ S ₂ : 1 = 1:3 ^[d]
1  1a	BuS-SBu		87 (75)	90 (78) ^[i]
2  1b	BuS-SBu		67 (60)	95 (81)
3  1c	BuS-SBu		60 (55)	85 (75)
4  1d	BuS-SBu		54 (48)	77 (71) ^[e]
5  1e	BuS-SBu		82 (75)	85 (80)
6  1f	BuS-SBu		63 (58) ^[f]	–
7  1g	BuS-SBu		74 (61)	–
8 1a	MeS-SMe		65 (55)	70 (60)
9 1g	MeS-SMe		85 (76)	92 (81)
10 1a	<i>i</i> PrS-S <i>i</i> Pr		72 (60)	76 (62)
11 1g	<i>i</i> PrS-S <i>i</i> Pr		68 (64)	95 (84)
12 1a	CyS-SCy		67 (60) ^[g]	95 (81) ^[e]
13 1g	CyS-SCy		75 (65) ^[g]	94 (87) ^[e]

[a] See experimental part for complete description of synthesis and isolation details. [b] NMR yield after completing the reaction and isolated yield after separation and purification (in parenthesis). [c] 100°, 2 h, solvent free (Method A; see Experimental Section). [d] 100°C, 1 h, solvent free (Method B; see Experimental Section). [e] Reaction time 2 h. [f] 80°C, 4 h, 0.5 mL of benzene (Method C; see Experimental Section). [g] Reaction time 4 h. [h] Stereoselectivity > 99:1. [i] The reaction on 10 mmol scale.

was carried out at 80°C in benzene (entry 6, Table 5). Compounds **2f** and **2g** were obtained in good isolated yields of 58–61%.

Other dialkyldisulfides, for example, Me₂S₂, *i*Pr₂S₂, and Cy₂S₂, were successfully used in the addition reaction (entries 8–13, Table 5). In the case of Cy₂S₂, a longer reaction time (4 h) was required to compensate for the lower reactivity of this bulky substrate.^[15]

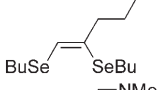
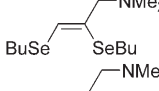
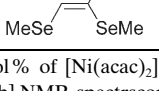
An important advantage of the developed synthetic procedure is the ability to scale up to greater amount of the product. Carrying out the catalytic reaction of **1a** and Bu₂S₂ at 10 mmol scale resulted in 90% NMR yield (78% isolated yield, > 2 g of **2a**). The reaction was carried out with the

same excellent stereoselectivity and with a slightly better yield with respect to the 1 mmol scale reaction (entry 1, Table 5).

In short, the developed catalytic system allows the addition dialkyldisulfides to alkynes in good isolated yields (58–87%) and excellent stereoselectivity (> 99:1). Rapid, dry column flash chromatography^[16] was successfully utilized for isolation and purification of all products throughout the study.^[17]

The synthetic procedure optimized for the addition of S–S bond to alkynes showed excellent results in the addition of the Se–Se bond (Table 6). The Ni-catalyzed addition of Bu₂Se₂ to **1a** and **1e** was carried out with high isolated yields of 87–88% (entries 1, 2; Table 6). Addition of Me₂Se₂ to **1e** was performed with 59% isolated yield (entry 3, Table 6). All the studied bis-selenation reactions were carried out with high stereoselectivity (*Z*:*E* > 99:1). Compared with the Ni-catalyzed bithiolation reaction discussed earlier, Ni-catalyzed Se–Se bond addition to alkynes suffers less from side reactions and high yields were obtained even at 1:1 ratio of the substrates (Table 6).

Table 6. Ni-catalyzed addition of Alk₂Se₂ to alkynes.^[a]

Alkyne	RSe-SeR	Product	Yield ^[b] [%]
1 1a	BuSe-SeBu		95 (87)
2 1e	BuSe-SeBu		95 (88)
3 1e	MeSe-SeMe		71 (59)

[a] Conditions: 100°C, 2 h, 3 mol% of [Ni(acac)₂], solvent free (Method A; see Experimental Section). [b] NMR spectroscopic yield after completing the reaction and isolated yield after separation and purification (in parenthesis).

Pd-catalyzed bsthioation and bis-selenation of alkynes:

The good results obtained for the Ni complexes led us to re-investigate the possibility of creating a catalytic system based on Pd. Most of the studied ligands did not result in good yields of **2a** in the model reaction of Bu₂S₂ addition to **1a**; selected representative examples are listed in Table 7 (entries 1–7). Surprisingly, introducing the bulky Cy group

Table 7. Ligand effect on the yield of **2a** in Pd-catalyzed reaction of Bu₂S₂ and 1-hexyne.^[a]

Ligand (L)	Yield [%]		
	solvent free	in benzene ^[b]	
1	PPh ₃	6	4
2	P(O <i>i</i> Pr) ₃	4	2
3	dppb	3	3
4	PEtPh ₂	3	3
5	PBu ₃	2	2
6	PMePh ₂	3	3
7	PMe ₂ Ph	2	2
8	PCy ₃	3	3
9	PCyPh ₂	8	6
10	PCy ₂ Ph	16	10

[a] Bu₂S₂ (1 mmol), 1-hexyne (1 mmol). [b] In benzene (0.5 mL).

to the phosphane ligand improved the performance of the catalytic reaction (entries 8–10, Table 7). The best result was achieved with the PCy₂Ph ligand—16% of **2a** after 2 h at 100 °C (entry 10, Table 7). Although in the case of Pd a much smaller difference was observed between the solvent-free reaction and that in solvent (Table 7), we have chosen solvent-free methodology for green chemistry reasons.

Pd-catalyzed transformation was much slower (16% of **2a**; entry 10, Table 7) compared to the Ni-catalyzed transformation (87% of **2a**; entry 13, Table 2) under the same conditions (100 °C, 2 h). However, in contrast to Ni-catalyzed reaction, longer heating and higher temperatures applied in the Pd catalytic system did not cause noticeable decrease in the product yield (Table 8). It was possible to carry out Pd-catalyzed reaction in the temperature range 100–200 °C with 16–80% yield of **2a** after 2 h (entries 1–5, Table 8). Further heating increased the yield upon complete conversion of the substrates.

In the case of Pd-catalyzed reaction the best yield was achieved with 45 mol% of the ligand (entries 1–4; Table 9).

Table 8. The yield of **2a** at different temperatures in Pd-catalyzed reaction.^[a]

	T [°C]	Yield [%]
1	100	16
2	120	26
3	140	44
4	160	64
5	200	80

[a] Bu₂S₂ (1 mmol), 1-hexyne (1 mmol), [Pd₂(dba)₃] (1.5 mol%), and PCy₂Ph (30 mol%), 2 h, solvent free.

Table 9. The yield of **2a** in Pd-catalyzed reaction with different amounts of the PCy₂Ph ligand.^[a]

	Ligand [mol %]	Yield [%]
1	15	49
2	30	76
3	45	95
4	60	90

[a] Bu₂S₂ (1 mmol), 1-hexyne (1 mmol), [Pd₂(dba)₃] (1.5 mol%), and a given amount of PCy₂Ph ligand (140 °C, 6 h).

However, taking into account that the Pd system does not suffer from high temperatures and longer reaction times, utilization of 30 mol% is also acceptable.

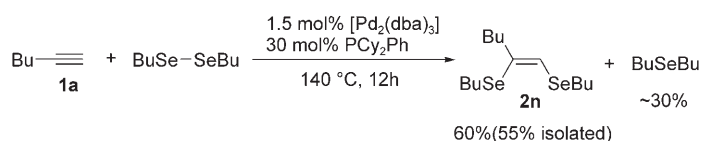
A practical and convenient synthetic procedure was developed for the Pd-catalyzed reaction at 140 °C^[18] for 12 h with 30 mol% of the ligand or at 140 °C for 6 h with 45 mol% of the ligand (Table 10). Excellent isolated yields of 83–89% and excellent stereoselectivity (>99:1) were observed at the ratio Bu₂S₂:alkyne = 1:1 as shown for the selected examples of **2a**, **2e**, and **2d** (entries 1–3, Table 10).

Table 10. Pd-catalyzed Alk₂S₂ addition to alkynes.^[a]

	Alkyne	RS–SR	Product	Yield ^[b] [%]
1	1a	BuS–SBu	2a	95 (85)
2	1e	BuS–SBu	2e	95 (89)
3	1d	BuS–SBu	2d	92 (83) ^[c]

[a] Conditions: [Pd₂(dba)₃] (1.5 mol%), PCy₂Ph (45 mol%), solvent free, 140 °C, 6 h (or PCy₂Ph (30 mol%), 140 °C, 12 h). [b] NMR spectroscopic yield after completing the reaction and isolated yield after separation and purification (in parenthesis). [c] Reaction time: 9 h (45 mol% of PCy₂Ph) or 18 h (30 mol% of PCy₂Ph).

An attempt to carry out catalytic Bu₂Se₂ addition to **1a** in Pd⁰/PCy₂Ph system resulted only in 60% yield of **2n** (55% isolated yield) and about 40% of **1a** remained unreacted (Scheme 3). Two-dimensional ¹H-⁷⁷Se HMQC NMR analysis of the reaction crude confirmed the presence of Bu₂Se (≈30%).



Scheme 3. Pd-catalyzed reaction of Bu₂Se₂ and **1a**.

³¹P{¹H} examination of the crude product indicated the formation of Se=PCy₂Ph, presumably from the following reaction: PCy₂Ph + Bu₂Se₂ → Se=PCy₂Ph + Bu₂Se, which also takes place under Pd-catalyzed conditions. To confirm this assumption we carried out the reaction with equimolar ratio of PCy₂Ph and Bu₂Se₂ in the absence of alkyne. After 6 h at 140 °C nearly complete conversion of the phosphane to Se=PCy₂Ph (≈95%) was detected by NMR spectroscopy.

X-ray structure determination of 2e, 2i, 2k, and 2m: The *Z* configuration of most of the products was determined by 2D NOESY NMR experiments and some representative cases were a subject of X-ray structure determination. For this purpose we have prepared oxalic salts of **2i**, **2e**, **2k**, and **2m** (crystallized from MeOH). The molecular structures are shown in Figure 1, along with the atom numbering schemes. Selected bond lengths and angles are listed in Table 11. The X-ray analysis confirmed the *Z* configuration of the double bonds and revealed several unusual structural and crystal packing features.

The salts comprise the ammonium sulfur-containing [(*RS*)HC=C(SR)CH₂NHMe₂]⁺ ions and the oxalic acid [HOOC-COO]⁻ ions forming tight ionic pairs by bifurcate hydrogen bonds between the amino-H atom of the cation and two oxygen atoms of the anion (Figure 1, Table 12). It is interesting to note that different oxygen atoms of the anion take part in the hydrogen-bonding interactions, namely, either the carbonyl and hydroxyl oxygen atoms (in the case of **2i** and **2m**) or the two carbonyl oxygen atoms (in the case of **2e**, **2k**, and **2m**). Remarkably, both types of hydrogen-bonding interaction were present simultaneously in the crystal of compound **2m** for the two independent ionic pairs. Furthermore, the bifurcate hydrogen bonds are mainly characterized by the asymmetrical arrangement of the amino-H atom relative to the two oxygen atoms, except for one of the two independent ionic pairs in compound **2m**, in which the amino-H atom is almost symmetrically located relative to the two oxygen atoms (Table 12). We have denoted this unusual ionic pair of compounds as **2m** and **2m***, because it possesses a number of the additional interesting properties discussed below. The asymmetrical arrangement of the amino-H atom relative to the two oxygen atoms in the bifurcate hydrogen bonds was also observed in the previously studied related compounds.^[4b,8c,9] Moreover, the OH group of one anion is bound up by the strong hydrogen bond with the negatively charged oxygen atom of another anion (Table 12).

The conformations of the cations and anions are worth mentioning. The cations of **2i**, **2e**, **2k**, and **2m** have a *Z* configuration,^[19] which is responsible for the structural features of the ionic pair **2m***. It turned out that in the ionic pair **2m***, the anion lies over the =C(H)SR fragment, whereas that in the other ionic pairs resides on the opposite side of the cation, over the -SR fragment (Figure 1). The arrangement of the terminal substituents at the two sulfur atoms relative to the C=C double bond in the cations is of particular interest. So, the substituent at the sulfur atom from the more crowded side of the cation is located *gauche* to the

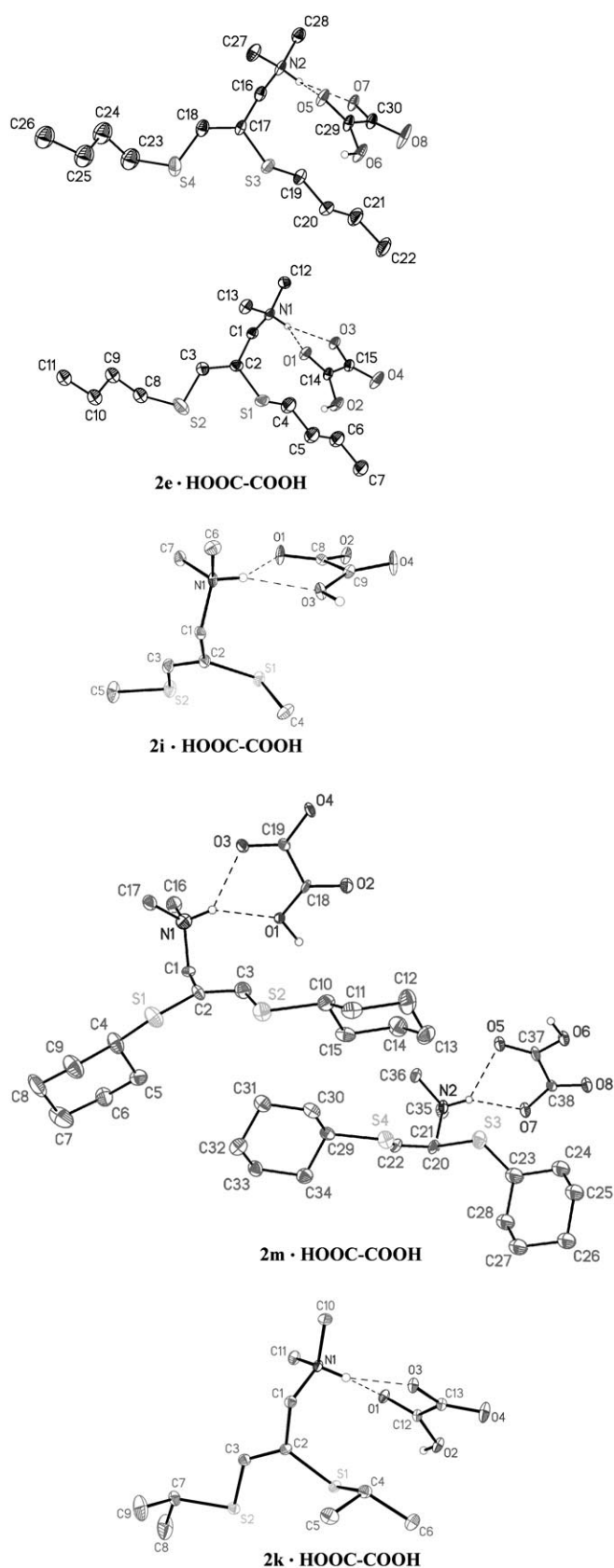


Figure 1. Molecular structures of oxalic salts of **2e**, **2i** (the two independent ionic pairs are shown; the alternative positions of the disordered butyl groups with less occupancies are not shown), **2m**, and **2k** (the two independent ionic pairs are shown; the alternative position of the disordered cyclohexyl group with less occupancy is not shown) depicting thermal ellipsoids at the 50% probability level; most hydrogen atoms are omitted for clarity; dash lines indicate the bifurcate hydrogen bonds.

Table 11. Selected bond lengths [Å] and angles [°] for **2i**, **2e**, **2k**, and **2m**.

compound 2i			
S1–C2	1.767(3)	C2–S1–C4	101.45(15)
S1–C4	1.815(3)	C3–S2–C5	99.27(15)
S2–C3	1.735(3)	C3–C2–S1	119.8(2)
S2–C5	1.805(3)	C2–C3–S2	126.2(2)
C2–C3	1.341(4)	C4–S1–C2–C3	–135.1(3)
		C5–S2–C3–C2	169.7(3)
compound 2e			
S1–C2	1.761(3)	C2–S1–C4	103.15(18)
S1–C4	1.809(5)	C3–S2–C8	99.93(17)
S2–C3	1.734(3)	C3–C2–S1	119.2(2)
S2–C8	1.811(4)	C2–C3–S2	124.5(3)
C2–C3	1.343(4)	C17–S3–C19	103.11(14)
S3–C17	1.764(3)	C18–S4–C23	102.1(2)
S3–C19	1.811(3)	C18–S4–C23'	93.7(3)
S4–C18	1.734(3)	C18–C17–S3	119.9(2)
S4–C23	1.8217	C17–C18–S4	125.0(2)
S4–C23'	1.857(8)	C4–S1–C2–C3	125.4(3)
C17–C18	1.334(4)	C8–S2–C3–C2	–162.03
		C19–S3–C17–C18	132.1(3)
		C23–S4–C18–C17	–154.4(3)
		C23'–S4–C18–C17	168.6(5)
compound 2k			
S1–C2	1.7665(9)	C2–S1–C4	102.64(4)
S1–C4	1.8329(10)	C3–S2–C7	99.20(5)
S2–C3	1.7390(10)	C3–C2–S1	120.57(7)
S2–C7	1.8326(11)	C2–C3–S2	125.90(8)
C2–C3	1.3429(13)	C4–S1–C2–C3	–136.15(8)
		C7–S2–C3–C2	176.10(9)
Compound 2m			
S1–C2	1.766(6)	C2–S1–C4	103.3(3)
S1–C4	1.799(7)	C3–S2–C10	100.2(3)
S2–C3	1.743(7)	C3–C2–S1	118.0(5)
S2–C10	1.806(7)	C2–C3–S2	124.1(5)
C2–C3	1.354(8)	C21–S3–C23	102.4(3)
S3–C21	1.754(6)	C22–S4–C29	100.3(3)
S3–C23	1.794(7)	C22–C21–S3	119.7(6)
S4–C22	1.731(7)	C21–C22–S4	126.1(5)
S4–C29	1.823(7)	C4–S1–C2–C3	–147.9(7)
C21–C22	1.338(8)	C10–S2–C3–C2	174.4(7)
		C23–S3–C21–C22	142.4(6)
		C29–S4–C22–C21	172.9(6)

C=C double bond, but the substituent at the sulfur atom from the less crowded side of the cation is located *trans* to this bond (Figure 1, Table 11).

It is known that the oxalic acid anion often has a twisted geometry in salts including different hydrogen bonds. Similar conformation of the anions is also found in **2i** (the twist angle is 21.0°), **2e** (the twist angles are 19.6 and 23.0° for the two independent anions), **2k** (the twist angle is 23.3°) and **2m** (the twist angle is 26.6°), except for the unusual ionic pair **2m***, in which the anion has a nearly planar conformation with the twist angle of only 6.3°. It should be noted that the planar oxalic acid anion was also revealed earlier in one of the cases,^[9] whereas in the other related structures^[4b,8c] it has the expected twisted conformation.

The crystal packing of compounds **2i**, **2e**, **2k**, and **2m** described in this paper (Figure 2) is built up by the alternate anion and cation layers. The anions bound in the chains by the O–H...O hydrogen bonds form sheets, while the amino

Table 12. Hydrogen bonds for **2i**, **2e**, **2k**, and **2m** [lengths in Å and angles in °].^[a]

D–H...A	d(D–H)	d(H...A)	d(D...A)	∠(DHA)
compound 2i				
N1–H1N...O1	0.92	1.93	2.764(3)	149
N1–H1N...O3	0.92	2.26	2.944(3)	131
O3–H3O...O2 ⁱ	0.97	1.50	2.468(2)	178
compound 2e				
N1–H1N...O1 ⁱⁱ	0.90	2.29	3.048(3)	141
N1–H1N...O3 ⁱⁱⁱ	0.90	2.03	2.790(3)	142
O2–H2O...O3 ⁱⁱⁱ	0.89	1.62	2.509(3)	179
N2–H2N...O5 ^{iv}	0.91	2.22	3.010(3)	144
N2–H2N...O7 ^{iv}	0.91	2.07	2.791(3)	135
O6–H6O...O7 ^v	0.88	1.60	2.485(3)	176
compound 2k				
N1–H1N...O1	0.88	2.29	3.0020(11)	138
N1–H1N...O3	0.88	2.01	2.7619(11)	142
O2–H2O...O3 ^{vi}	0.99	1.52	2.5104(9)	176
compound 2m				
N1–H1N...O1	0.93	2.17	2.901(7)	135
N1–H1N...O3	0.93	2.11	2.879(8)	139
O1–H1O...O4 ^{vii}	0.99	1.53	2.480(8)	160
N2–H2N...O5	0.93	2.26	3.004(7)	137
N2–H2N...O7	0.93	1.99	2.776(7)	141
O6–H6O...O7 ^{viii}	0.91	1.60	2.486(7)	167

[a] Symmetry transformations used to generate equivalent atoms: i: x, y–1, z; ii: x–1, –y+1, z–1/2; iii: x, –y+1, z+1/2; iv: x–1, y, z; v: x, –y, z+1/2; vi: x, –y+3/2, z–1/2; vii: –x+3/2, y, z+1/2; viii: –x+3/2, y, z–1/2.

groups of the cations separate the anion chains from each other within the sheets. The cation sheets are formed by sulfide parts of the cations and are located between the anion sheets. However, the alternation of the anion and cation layers in **2i** occurs in pairs,^[20] that is, two adjusted anion layers are located between two adjusted cation layers, whereas in **2e**, **2k**, **2m** the structures are built up by the alternation of one anion layer and two cation layers.^[19]

Apparently, both the unusual structure of the ionic pair **2m*** and the different crystal packing are determined by the spatial size of the terminal –SR substituents at the C=C double bond. Indeed, the pairwise alternation of the anion and cation layers in **2i** can be explained by the small spatial size of the –SMe substituents; in the literature such structures have only been observed in the absence of the second –SR substituent at the C=C double bond.^[20] On the other hand, the presence of the two bulky –SCy substituents at the C=C double bond in the structure of **2m** gives rise to the two independent ionic pairs of the different configurations to form the crystal of high density.

Crystal structures of vinylchalcogenides with carboxylic group provide an important information concerning non-bonded X...O interactions (X=S, Se). Such interactions are of great importance for understanding of the mechanism of biological action of chalcogen-containing species^[21] as well as for structural investigations.^[22] The present compounds possess unusual structure and bonding properties compared to the molecules studied earlier and provide important information for future studies of this phenomenon.

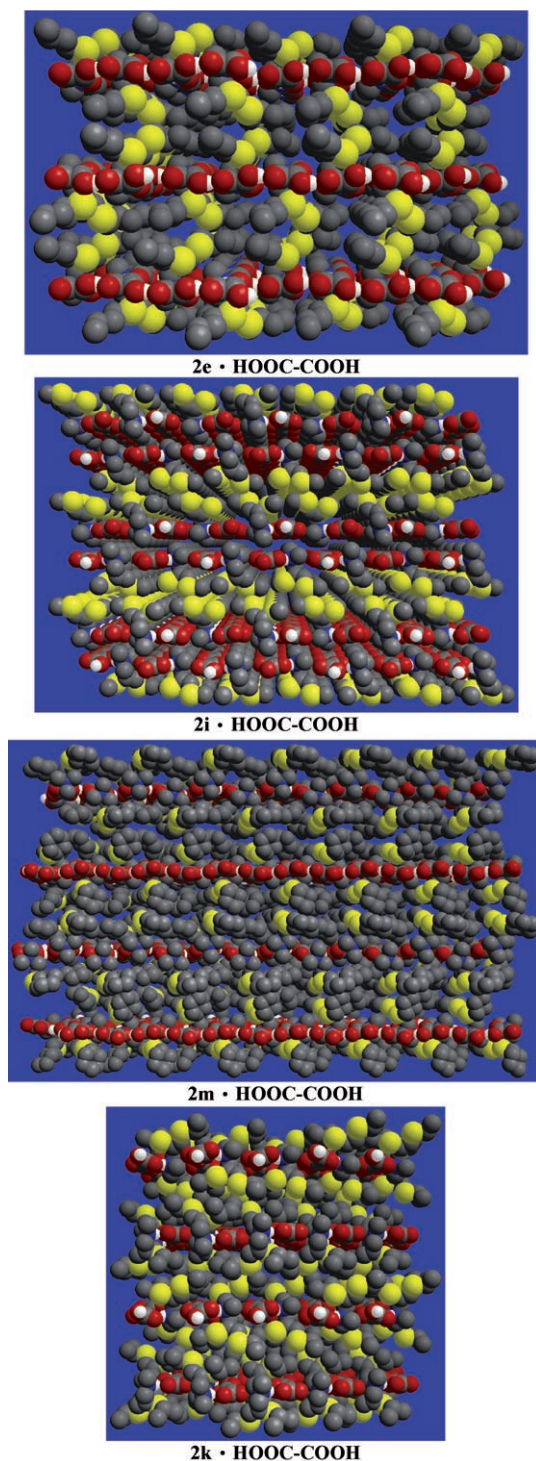
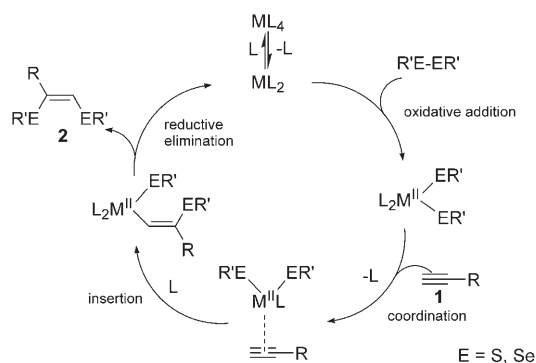


Figure 2. Crystal packing of oxalic salts of **2e**, **2i**, **2m**, and **2k**.

Discussion

A plausible catalytic reaction mechanism involves the following steps (Scheme 4): 1) oxidative addition of E–E bond to M^0 , 2) alkyne coordination to the metal center, 3) alkyne insertion into the M–E bond, and 4) C–E reductive elimination leading to the product **2** and regeneration of M^0 .



Scheme 4. Plausible mechanism of the catalytic reaction.

According to experimental studies, oxidative addition of an E–E bond to a low-valent-metal complex may result in a diverse range of product depending on metal and ligand type.^[3,23] Oxidative addition of diaryldichalcogenides to Pd^0 led to a mixture of *trans* and *cis* mono- and dinuclear complexes detected by ^{31}P NMR spectroscopy.^[4c] It was shown that an excess of phosphane ligand is required to suppress polymerization of Pd complexes and avoid formation of catalytically inactive $[[Pd(SR)_2]_n]$ species.^[4c,3] Probably, a similar effect was observed in the studied Ni system, which also required an excess of the ligand to achieve good product yields. Unfortunately, for the Ni-based catalytic system we were unable to obtain high-quality ^{31}P NMR spectra due to very broad lines.^[24]

Theoretical studies of the oxidative addition of $AlkS-SAlk$ and $AlkSe-SeAlk$ to Pd^0 have been performed earlier,^[25] however, no data is available concerning the reactivity of the Ni complexes. To reveal relative reactivity of Pd and Ni complexes in E–E and C–E bond oxidative addition, we have carried out a series of theoretical calculations on the model reactions (Figure 3).

Starting from the initial point $ML_2 + R_2E_2$ (**I**) the first step is coordination of the chalcogen atom to the metal center. For $M=Pd$ this step is exothermic by $\Delta H = -2.3$ and -3.6 kcal mol⁻¹ for $E=S$ and Se , respectively (Table 13).^[26] For $M=Ni$ much stronger binding of R_2E_2 was calculated $\Delta H = -13.1$ and -13.5 kcal mol⁻¹ for $E=S$ and Se , respectively. Optimized Pd–E1 bond lengths in **II** are 2.433 and 2.519 Å; optimized Ni–E1 bond lengths in **II** are 2.143 and 2.262 Å for $E=S$ and Se , respectively (Table 14). It is important to note that stronger binding in the case of Ni caused considerable elongation of the E1–E2 bond in **II**: 2.174 and 2.442 Å, compared to 2.128 and 2.398 Å for Pd ($E=S$ and Se , respectively). Thus, R_2E_2 coordination to the NiL_2 complex results in significant elongation (and most likely weakening) of the E–E bond compared to PdL_2 .

Starting from the complex **II** the reaction may proceed either by an E–E oxidative addition pathway **II**→**III-TS**→**IV** or a C–E oxidative addition pathway **II**→**V-TS**→**VI** (Figure 3). Let us consider the former pathway first.

In the case of Pd symmetric three-centered transition state was located, movement along the reaction coordinate

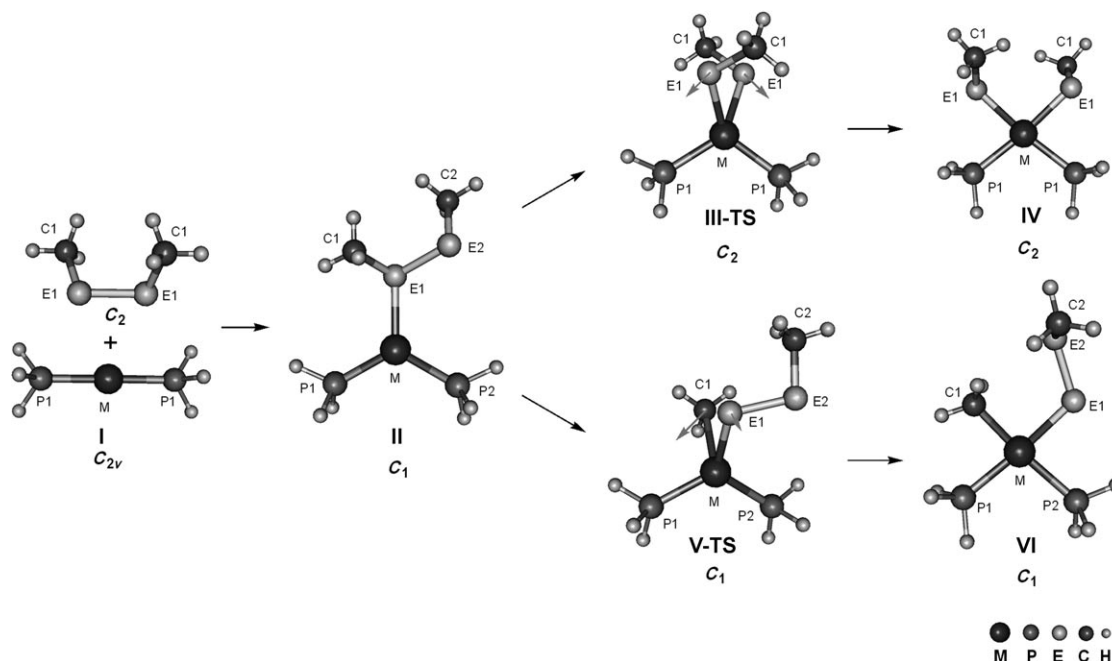


Figure 3. B3LYP/SDD 6-311G(d) optimized molecular structures of **I–VI** with atom numbering and converged symmetry point groups (in bold).

Table 13. Calculated ΔE , ΔH , and ΔG energy surfaces [in kcal mol⁻¹] of the E–E and E–C oxidative addition reaction (E = S, Se) to M(PH₃)₂ at B3LYP/SDD 6-311G(d) level for M = Pd and Ni.^[a]

	M = Ni		M = Pd	
	E = S	E = Se	E = S	E = Se
I	0.0/0.0/0.0	0.0/0.0/0.0	0.0/0.0/0.0	0.0/0.0/0.0
II	-14.2/-13.1/-2.4	-14.6/-13.5/-2.6	-3.1/-2.3/6.5	-4.5/-3.6/5.6
III-TS	-/-/-	-/-/-	9.9/9.9/20.8	3.6/3.8/15.5
IV	-34.3/-32.4/-19.2	-29.1/-27.1/-13.8	-14.5/-12.9/-0.1	-12.6/-10.9/2.2
V-TS	3.3/2.5/14.8	-1.1/-1.6/11.1	26.7/25.8/36.4	20.3/19.7/30.5
VI	-16.5/-15.7/-3.2	-18.1/-17.0/-4.2	0.7/1.3/13.4	-2.3/-1.4/11.0

[a] Calculated data on energy, enthalpy, and free energy is given in the order *E/H/G* for each case.

involves elongation and breakage of the E–E bond and formation of two new M–E bonds (Figure 3). The activation barriers for the reaction are $\Delta H^\ddagger = 12.2$ and 7.4 kcal mol⁻¹ for E = S and Se, respectively (Table 13). The oxidative addition step is exothermic by $\Delta H = -6.6$ and -3.4 kcal mol⁻¹ mol for E = S and Se, respectively. A rather long M–E bond length in **III-TS** (Table 14) confirms the earlier character of the transition state in agreement with energetic data (Table 13). On the ΔG surface the activation barriers are $\Delta G^\ddagger = 20.8$ and 15.5 kcal mol⁻¹[27] and the oxidative addition step was nearly thermo neutral or endoergic, $\Delta G = -0.1$ and 2.2 kcal mol⁻¹ for E = S and Se, respectively.

In the case of Ni complex oxidative addition of the E–E bond took place as a barrierless reaction^[28] and was significantly more exothermic $\Delta H = -16.8$ and -11.2 kcal mol⁻¹ for E = S and Se, respectively. On the ΔG surface the reaction is favorable in energy by 19.2 and 13.8 kcal mol⁻¹ compared to **I** and by 16.8 and 11.2 kcal mol⁻¹ compared to **II** for E = S and Se, respectively.

The second pathway—C–E oxidative addition—proceeds via the **V-TS** transition state, starting from complex **II**

(Figure 3). The calculated activation barriers for M = Pd are $\Delta H^\ddagger = 28.1$ and 23.3 kcal mol⁻¹; for the same step involving Ni complexes the calculated activation barriers are $\Delta H^\ddagger = 15.6$ and 11.9 kcal mol⁻¹ (for E = S and Se, respectively). According to the length of M–E bond in **V-TS** and **III-TS**, the former transition state possesses more late character (see

Table 14) in agreement with higher activation barriers.

From a kinetic point of view Ni complexes should be more reactive with respect to Pd in C–E bond oxidative addition leading to **VI**. However, according to thermodynamic properties the energy difference between the complexes **IV** and **VI** is more favorable towards formation **IV** in the case of Ni (on ΔH surface **IV** is more stable than **VI** by 16.7 and 10.1 kcal mol⁻¹ for M = Ni and by 14.2 and 9.5 kcal mol⁻¹ for M = Pd; see Table 13).

The following conclusions concerning the relative reactivity of the studied transition metal complexes can be emphasized:

- 1) NiL₂ complexes are more reactive in E–E bond oxidative addition than PdL₂.
- 2) For both metals E–E bond oxidative addition is energetically more favorable than C–E bond oxidative addition.
- 3) The activation of C–E bond by transition metal complexes should be more easy for E = Se compared to E = S.^[29]

Table 14. Optimized geometry parameters [bond lengths in Å, angles in °] of structures **I–VI** corresponding to the E–E and E–C oxidative addition reaction (E=S, Se) to M(PH₃)₂ calculated at the B3LYP/SDD 6-311G(d) level for M=Pd and Ni (see Figure 3 for atom numbering).^[a]

	M	E	M–P1	M–P2	M–E1	M–C1	E1–E2	E1–C1	E2–C2	P1–M–P2
I	Ni	S	2.115	–	–	–	2.094	1.832	–	180.0
		Se	2.115	–	–	–	2.355	1.982	–	180.0
	Pd	S	2.289	–	–	–	2.094	1.832	–	180.0
		Se	2.115	–	–	–	2.355	1.982	–	180.0
II	Ni	S	2.136	2.155	2.143	–	2.174	1.841	1.831	117.6
		Se	2.139	2.162	2.262	–	2.442	1.989	1.980	117.0
	Pd	S	2.305	2.330	2.433	–	2.128	1.837	1.832	121.1
		Se	2.311	2.336	2.519	–	2.398	1.985	1.981	120.6
III-TS	Pd	S	2.387	–	2.419	–	2.454	1.834	–	112.0
		Se	2.388	–	2.518	–	2.669	1.984	–	112.0
IV	Ni	S	2.218	–	2.246	–	–	1.837	–	100.6
		Se	2.214	–	2.367	–	–	1.983	–	99.6
	Pd	S	2.337	–	2.388	–	–	1.837	–	104.0
		Se	2.340	–	2.504	–	–	1.982	–	103.3
V-TS	Ni	S	2.204	2.216	2.102	2.069	2.134	2.215	1.832	118.2
		Se	2.202	2.219	2.224	2.067	2.399	2.328	1.981	117.5
	Pd	S	2.376	2.410	2.312	2.290	2.106	2.354	1.832	118.4
		Se	2.383	2.413	2.412	2.283	2.373	2.474	1.982	119.0
VI	Ni	S	2.181	2.271	2.227	1.962	2.099	–	1.830	97.8
		Se	2.182	2.260	2.348	1.966	2.365	–	1.980	97.1
	Pd	S	2.317	2.415	2.379	2.093	2.090	–	1.830	99.6
		Se	2.323	2.406	2.494	2.099	2.357	–	1.981	99.6

[a] Imaginary frequencies for the transition states: **III-TS** (Pd, S)=171i cm⁻¹, **III-TS** (Pd, Se)=77i cm⁻¹, **V-TS** (Ni, S)=299i cm⁻¹, **V-TS** (Ni, Se)=228i cm⁻¹, **V-TS** (Pd, S)=281i cm⁻¹, **V-TS** (Pd, Se)=226i cm⁻¹.

The results of the theoretical study are in excellent agreement with experimental findings and explain several important points. Particularly, relative reactivity of Pd and Ni complexes in E–E oxidative reaction is in agreement with observed reactivity of these complexes in the catalytic reaction. Smaller activation barriers and more stable products of the E–E bond oxidative addition compared to C–E bond explains high selectivity of transition-metal-catalyzed transformation towards the R₂E₂ substrate (see Scheme 2 and corresponding discussion). Relative reactivity of sulfur and selenium compounds in C–E bond activation provides necessary basis for understanding why the side reaction leading to R₂E was observed only in the case of E=Se (see Scheme 3 and corresponding discussion). According to the theoretical study, the oxidative addition of S–S and Se–Se bonds to PdL₂ and NiL₂ complexes is characterized by relatively small activation barriers, therefore, it may not be considered as a rate-determining step.

The next step after completing the oxidative addition is alkyne insertion into the M–E bond (Scheme 4). By experimental^[30] and theoretical studies^[31] it was shown that alkyne insertion into the M–E bond takes place with high stereoselectivity and is responsible for overall stereoselectivity of the catalytic cycle (providing that *Z/E* isomerization of the product double bond and noncatalytic addition reactions are avoided). In this case, only *Z* configuration of the double bond should be expected as a result of *syn*-addition. High stereoselectivity in the studied system (*Z:E* >99:1) confirmed by NMR spectroscopy and X-ray studies is in agreement with proposed reaction mechanism. The last step of the catalytic cycle, reductive elimination (Scheme 4), is

known in the framework of catalytic heterofunctionalization reactions and corresponding discussion will not be repeated here.^[2]

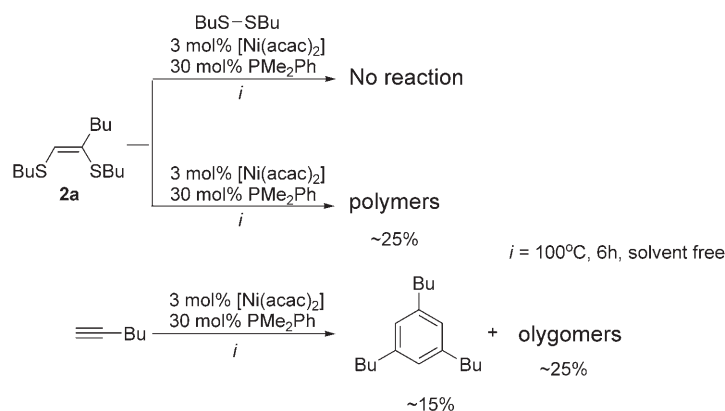
On the basis of our study we can suggest a plausible mechanism of the catalytic reaction. However, at the moment we cannot clearly say which step of the catalytic cycle is responsible for the observed ligand effect. In addition to intrinsic stabilization (or destabilization) of transition-metal intermediates by the ligand, the second important factor is ligand dissociation (or association) in each step of the catalytic cycles, which significantly complicates the overall picture. Further studies are required to reveal mechanistic details of the developed catalytic system.

An important question is the nature of the side reactions

that take place in the studied system. To find an answer we have carried out the reactions of pure product **2a** under different conditions. These reactions model possible transformations of the product under catalytic conditions.

No reaction took place between the **2a** and Bu₂S₂ in the Ni/PMe₂Ph system after 6 h at 100 °C (Scheme 5), but if **2a** was heated in the presence of Ni/PMe₂Ph (without Bu₂S₂) broad signals in ¹H NMR spectrum appear at δ=6.0 and 6.5 ppm, suggesting that polymerization of **2a** took place. Therefore, under catalytic conditions at the end of reaction (when Bu₂S₂ is consumed) the product can be converted to a polymer.

Heating of **1a** in Ni/PMe₂Ph system resulted in the formation of 1,3,5-tributylbenzene (¹H δ_{Ar}=7.2 ppm) and oligomeric species (several signals in the range δ=5.5–4.5 ppm).



Scheme 5.

Triple-bond trimerization and oligomerization catalyzed by Ni complexes are well-known reactions,^[32] which also took place under the studied reaction conditions.

If Pd catalytic system was utilized instead of Ni neither decomposition of **2a** nor oligomerization of the alkyne were observed.

These results are in excellent agreement with the findings concerning catalytic system described earlier. Thus, it became clear why an excess of alkyne might be required to complete conversion of R_2E_2 in Ni-catalyzed transformation (but not for Pd case) and the reason for a decrease of the product yield if reaction time is overestimated.

Conclusions

We have developed two novel catalytic systems based on Pd and Ni complexes, which solved the problem of stereoselective addition of dialkyldichalcogenides to alkynes (60–90% yields and $Z:E > 99:1$ selectivity). The choice of the ligand was the key finding to carry out the reaction: PMe_2Ph was the optimal ligand for the Ni catalytic system and PCy_2Ph was the optimal ligand for the Pd catalytic system. In both Ni and Pd catalytic systems an excess of the ligand was required to achieve high product yields.

Ni catalyst has several important advantages: 1) superior catalytic activity, 2) high stereoselectivity, 3) low cost, 4) relatively mild reaction conditions (100°C, 2 h), and 5) good yields for both $E=S$ and Se . The disadvantages of the Ni system include side reactions involving alkyne (for $E=S$, but not for $E=Se$) and decomposition of the product at the end of reaction. Careful optimizations of reaction conditions minimized the influence of these drawbacks on the efficiency of the synthetic procedure.

The Pd catalyst was significantly less active and required higher temperature and longer time (140°C, 12 h). As a result, Pd/ PCy_2Ph catalytic system has a narrow scope and was applicable only for the addition of dialkyldisulfides to alkynes. The low catalytic activity of Pd required more harsh reaction conditions leading to decomposition of dialkyldiselenide. However, an important advantage of the Pd system is an absence of the side reactions involving the alkyne (for both $E=S$ and Se).

Experimental Section

General: Unless otherwise noted, the synthetic work was carried out under argon atmosphere. $[Pd_2(dba)_3]$ (dba = dibenzylideneacetone) was prepared according to a published procedure.^[33] Bu_2Se_2 was prepared according to a modified literature procedure (see below). Other reagents were obtained from Acros and Lancaster and used as supplied (checked by NMR spectroscopy before use). $[Ni(acac)_2]$ was dried under vacuum (0.1–0.05 Torr, 60°C, 30 min) before use. Solvents were purified according to published methods. The reaction was carried out in PTFE screw capped tubes or flasks.

All NMR measurements were performed using a three channel Bruker DRX-500 spectrometer operating at 500.1, 202.5, 125.8 and 95.4 MHz for

1H , ^{31}P , ^{13}C , and ^{77}Se nuclei, respectively. The spectra were processed on a PC Linux workstation using XWINMR software package. All 2D spectra were recorded by using an inverse triple resonance probe head with active shielded Z-gradient coil. 1H and ^{13}C chemical shifts are reported relative to the corresponding solvent signals used as internal reference, external $Ph_2Se_2/CDCl_3$ ($\delta = 463.0$ ppm) and H_3PO_4/H_2O was used for ^{77}Se and ^{31}P , respectively. 2D 1H - ^{77}Se HMQC and NOESY NMR experiments were carried out as described previously.^[4a,34]

General procedure for the Ni-catalyzed synthesis of **2a–2p**

Method A: $[Ni(acac)_2]$ (3.0×10^{-5} mol, 7.7 mg), R_2E_2 (1.0×10^{-3} mol) and PMe_2Ph (3.0×10^{-4} mol, 41.5 mg) were placed in a reaction vessel and stirred at room temperature until a homogeneous brown solution was formed (ca. 5–10 min). The alkyne (1.0×10^{-3} mol) was added to the solution and the reaction was carried out at 100°C under stirring until complete conversion of the R_2E_2 (2 h for most substrates; see Tables 5 and 6).^[35]

Method B: The same as Method A except 3.0×10^{-3} mol of the alkyne was added (1 h for most substrates; see Tables 5 and 6).^[35]

Method C: The same as Method A except that reaction was carried out in benzene (0.5 mL), which was placed into the reaction vessel first, followed by compounds in the order: R_2E_2 , PMe_2Ph , $[Ni(acac)_2]$, alkyne (see Table 5).^[35]

General procedure for the Pd-catalyzed synthesis of **2a, **2e**, **2d**:** $[Pd_2(dba)_3]$ (1.5×10^{-5} mol, 15.5 mg), R_2E_2 (1.0×10^{-3} mol) and PCy_2Ph (3.0×10^{-4} mol, 82.3 mg) were placed in a reaction vessel and stirred at room temperature until a homogeneous dark-brown solution was formed (ca. 5–10 min). The alkyne (1.0×10^{-3} mol) was added to the solution and the stirring was continued for additional 10 min. The reaction was carried out at 140°C under stirring until complete conversion of the R_2E_2 (12–18 h, see Table 10).

Isolation and characterization: After completion of the reaction, the products were purified by dry column flash chromatography on silica.^[6] For the compounds **2e**, **2i**, **2k**, **2m**, **2o**, and **2p** hexane/ethylacetate gradient elution was applied (prior to chromatography the silica was washed by a solution of 5–6 drops of Et_3N in 20 mL of hexane). For the other compounds hexane/toluene gradient elution was used. After drying in vacuum the pure products were obtained. The isolated yields given below were calculated based on initial amount of the R_2E_2 .

(1Z)-1,2-Bis(butylsulfanyl)-1-hexene (2a): Yellow oil; method A: 75% (0.200 g), method B: 80% (0.216 g); 1H NMR (500 MHz, $CDCl_3$): $\delta = 0.91$ (m, 9H), 1.32 (m, 2H), 1.40–1.65 (m, 10H), 2.25 (t, $J = 7.6$ Hz, 2H), 2.68 (t, $J = 7.5$ Hz, 4H), 6.05 ppm (s, 1H); $^{13}C\{^1H\}$ NMR (126 MHz, $CDCl_3$): $\delta = 13.56$, 13.59, 13.81, 21.66, 21.83, 21.97, 30.68, 30.97, 31.91, 32.35, 33.71, 36.55, 126.74, 131.98 ppm; MS (EI): m/z (%): 260 (18) $[M]^+$; elemental analysis calcd (%) for $C_{14}H_{28}S_2$: C 64.55, H 10.83, S 24.62; found: C 64.48, H 10.94, S 24.41.

[(Z)-1,2-Bis(butylsulfanyl)ethenyl]benzene (2b): Light yellow oil; method A: 60% (0.164 g), method B: 81% (0.240 g). Identified according to the published data.^[5]

(1Z)-1,2-Bis(butylsulfanyl)-3-methoxy-1-propene (2c): Light yellow oil; method A: 55% (0.133 g), method B: 75% (0.198 g); 1H NMR (500 MHz, $CDCl_3$): $\delta = 0.84$ (m, 6H), 1.36 (m, 4H), 1.49 (quintet, $J = 7.2$, 7.7 Hz, 2H), 1.56 (quintet, $J = 7.2$, 7.7 Hz, 2H), 2.66 (t, $J = 7.4$ Hz, 2H), 2.70 (t, $J = 7.4$ Hz, 2H), 3.25 (s, 3H), 3.94 (s, 2H), 6.36 ppm (s, 1H); $^{13}C\{^1H\}$ NMR (126 MHz, $CDCl_3$): $\delta = 13.36$, 13.40, 21.42, 21.62, 31.03, 31.85, 32.27, 33.50, 57.18, 75.18, 126.41, 131.69 ppm; MS (EI): m/z (%): 248 (39) $[M]^+$; elemental analysis calcd (%) for $C_{12}H_{24}OS_2$: C 58.01, H 9.74, S 25.81; found: C 58.25, H 9.91, S 25.49.

[(Z)-1,2-Bis(butylsulfanyl)ethenyl](trimethyl)silane (2d): Colorless oil; method A: 48% (0.120 g), method B: 71% (0.195 g). Identified according to the published data.^[5]

N-[(2Z)-2,3-Bis(butylsulfanyl)-2-propenyl]-N,N-dimethylamine (2e): Light yellow oil; method A: 75% (0.183 g), method B: 80% (0.208 g); 1H NMR (500 MHz, $CDCl_3$): $\delta = 0.88$ (m, 6H), 1.39 (m, 4H), 1.53 (quintet, $J = 7.4$ Hz, 2H), 1.59 (quintet, $J = 7.4$ Hz, 2H), 2.18 (s, 6H), 2.69 (t, $J = 7.4$ Hz, 2H), 2.76 (t, $J = 7.4$ Hz, 2H), 2.97 (s, 2H), 6.26 ppm (s, 1H); $^{13}C\{^1H\}$ NMR (126 MHz, $CDCl_3$): $\delta = 13.60$, 13.65, 21.66, 21.93, 30.96,

32.09, 32.49, 33.77, 44.99, 65.24, 128.29, 130.32 ppm; MS (EI): m/z (%): 261 (5) $[M]^+$; elemental analysis calcd (%) for $C_{13}H_{27}NS_2$: C 59.71, H 10.41, N 5.36, S 24.52; found: C 59.60, H 10.53, N 5.57, S 24.33.

(3Z)-3,4-Bis(butylsulfanyl)-2-methyl-3-buten-2-ol (2f): Light yellow oil; method C: 58% (0.151 g); 1H NMR (500 MHz, $CDCl_3$): δ = 0.93 (m, 6H), 1.41 (s, 6H), 1.41–1.46 (m, 4H), 1.59 (quintet, J = 7.1, 7.5 Hz, 2H), 1.64 (quintet, J = 7.1, 7.5 Hz, 2H), 2.74 (t, J = 7.3 Hz, 2H), 2.79 (t, J = 7.3 Hz, 2H), 6.73 ppm (s, 1H); $^{13}C\{^1H\}$ NMR (126 MHz, $CDCl_3$): δ = 13.40, 13.47, 21.49, 21.80, 29.05, 31.68, 32.35, 33.36, 33.61, 74.27, 133.50, 136.73 ppm; MS (EI): m/z (%): 262 (48) $[M]^+$; elemental analysis calcd (%) for $C_{13}H_{26}OS_2$: C 59.49, H 9.98, S 24.43; found: C 59.39, H 10.08, S 24.43.

1-[(Z)-1,2-Bis(butylsulfanyl)ethenyl]cyclohexanol (2g): Light yellow oil; method B: 61% (0.160 g); 1H NMR (500 MHz, $CDCl_3$): δ = 0.93 (m, 6H), 1.20 (m, 1H), 1.43 (m, 4H), 1.53–1.74 (m, 13H), 2.07 (s, 1H), 2.74 (t, J = 7.5 Hz, 2H), 2.78 (t, J = 7.5 Hz, 2H), 6.72 ppm (s, 1H); $^{13}C\{^1H\}$ NMR (126 MHz, $CDCl_3$): δ = 13.53, 13.61, 21.65, 21.99, 22.02, 25.43, 31.89, 32.52, 33.56, 33.95, 36.48, 75.00, 134.19, 137.51 ppm; MS (EI): m/z (%): 284 (18) $[M-H_2O]^+$; elemental analysis calcd (%) for $C_{16}H_{30}OS_2$: C 63.52, H 9.99, S 21.20; found: C 63.80, H 9.99, S 21.03.

(1Z)-1,2-Bis(methylsulfanyl)-1-hexene (2h): Light yellow oil; method A: 55% (0.100 g), method B: 60% (0.110 g); 1H NMR (500 MHz, $CDCl_3$): δ = 0.92 (t, J = 7.2 Hz, 3H), 1.33 (m, 2H), 1.50 (quintet, J = 7.4, 7.9 Hz, 2H), 2.25 (s, 3H), 2.28 (t, J = 7.2 Hz, 2H), 2.30 (s, 3H), 5.95 ppm (s, 1H); $^{13}C\{^1H\}$ NMR (126 MHz, $CDCl_3$): δ = 13.83, 14.51, 17.26, 21.98, 30.64, 35.73, 125.71, 133.25 ppm; elemental analysis calcd (%) for $C_8H_{16}S_2$: C 54.49, H 9.15, S 36.37; found: C 54.56, H 9.48, S 36.45; MS (EI): m/z (%): 176 (26) $[M]^+$.

N-[(2Z)-2,3-Bis(methylsulfanyl)-2-propenyl]-N,N-dimethylamine (2i): Light yellow oil; method A: 76% (0.140 g), method B: 81% (0.148 g); 1H NMR (500 MHz, $CDCl_3$): δ = 2.22 (s, 6H), 2.33 (s, 3H), 2.34 (s, 3H), 3.02 (s, 2H), 6.17 ppm (s, 1H); $^{13}C\{^1H\}$ NMR (126 MHz, $CDCl_3$): δ = 13.96, 16.92, 44.57, 64.15, 128.63, 129.28 ppm; MS (EI): m/z (%): 177 (13) $[M]^+$; elemental analysis calcd (%) for $C_7H_{15}NS_2$: C 47.41, H 8.53, N 7.90, S 36.16; found: C 47.54, H 8.37, N 7.81, S 35.93.

(1Z)-1,2-Bis(isopropylsulfanyl)-1-hexene (2j): Light yellow oil; method A: 60% (0.143 g), method B: 62% (0.146 g); 1H NMR (500 MHz, $CDCl_3$): δ = 0.92 (t, J = 7.0 Hz, 3H), 1.26 (d, J = 6.7 Hz, 6H), 1.31 (d, J = 6.7 Hz, 6H), 1.32 (m, 2H), 1.52 (quintet, J = 7.2, 7.6 Hz, 2H), 2.27 (t, J = 7.3 Hz, 2H), 3.09 (m, 1H), 3.31 (m, 1H), 6.22 ppm (s, 1H); $^{13}C\{^1H\}$ NMR (126 MHz, $CDCl_3$): δ = 13.75, 21.94, 23.23, 23.54, 30.65, 35.09, 37.26, 37.66, 127.52, 132.11 ppm; MS (EI): m/z (%): 232 (67) $[M]^+$; elemental analysis calcd (%) for $C_{12}H_{24}S_2$: C 62.00, H 10.41, S 27.59; found: C 62.11, H 10.57, S 27.54.

N-[(2Z)-2,3-Bis(isopropylsulfanyl)-2-propenyl]-N,N-dimethylamine (2k): Light yellow oil; method A: 64% (0.154 g), method B: 84% (0.205 g); 1H NMR (500 MHz, $CDCl_3$): δ = 1.26 (d, J = 6.5 Hz, 6H), 1.33 (d, J = 6.5 Hz, 6H), 2.23 (s, 6H), 3.02 (s, 2H), 3.14 (m, 1H), 3.45 (m, 1H), 6.51 ppm (s, 1H); $^{13}C\{^1H\}$ NMR (126 MHz, $CDCl_3$): δ = 23.33, 23.67, 35.33, 37.36, 45.07, 66.24, 127.90, 131.53 ppm; MS (EI): m/z (%): 233 (48) $[M]^+$; elemental analysis calcd (%) for $C_{11}H_{23}NS_2$: C 56.60, H 9.93, N 6.00, S 27.47; found: C 56.27, H 9.79, N 6.17, S 27.23.

[[[(Z)-1-Butyl-2-(cyclohexylsulfanyl)ethenyl]sulfanyl]cyclohexane (2l): Yellow oil; method A: 60% (0.192 g), method B: 81% (0.269 g); 1H NMR (500 MHz, $CDCl_3$): δ = 0.92 (t, J = 7.4 Hz, 3H), 1.20–1.44 (m, 12H), 1.51 (quintet, J = 7.4 Hz, 2H), 1.61 (m, 2H), 1.77 (m, 4H), 1.92 (m, 2H), 1.99 (m, 2H), 2.25 (t, J = 7.7 Hz, 2H), 2.82 (m, 1H), 3.02 (m, 1H), 6.22 ppm (s, 1H); $^{13}C\{^1H\}$ NMR (126 MHz, $CDCl_3$): δ = 13.84, 22.01, 25.59, 25.73, 25.98, 26.00, 30.74, 33.56, 33.77, 37.73, 43.50, 45.76, 127.50, 131.12 ppm; MS (EI): m/z (%): 312 (37) $[M]^+$; elemental analysis calcd (%) for $C_{18}H_{32}S_2$: C 69.16, H 10.32, S 20.52; found: C 69.07, H 10.58, S 20.38.

N-[(2Z)-2,3-Bis(cyclohexylsulfanyl)-2-propenyl]-N,N-dimethylamine (2m): Light yellow oil; method A: 65% (0.211 g), method B: 87% (0.288 g); 1H NMR (500 MHz, $CDCl_3$): δ = 1.13–1.41 (m, 10H), 1.54 (m, 2H), 1.70 (m, 4H), 1.86 (m, 2H), 1.93 (m, 2H), 2.15 (s, 6H), 2.80 (m, 1H), 2.93 (s, 2H), 3.10 (m, 1H), 6.43 ppm (s, 1H); $^{13}C\{^1H\}$ NMR (126 MHz, $CDCl_3$): δ = 25.38, 25.58, 25.78, 33.41, 33.67, 43.44, 44.93,

45.58, 66.19, 126.73, 131.47 ppm; MS (EI): m/z (%): 313 (11) $[M]^+$; elemental analysis calcd (%) for $C_{17}H_{31}NS_2$: C 65.12, H 9.96, N 4.47, S 20.45; found: C 64.89, H 10.00, N 4.59, S 20.24.

(1Z)-1,2-Bis(butylselanyl)-1-hexene (2n): Light yellow oil; 87% (0.300 g); 1H NMR (500 MHz, $CDCl_3$): δ = 0.92 (m, 9H), 1.31 (m, 2H), 1.42 (m, 4H), 1.51 (m, 2H), 1.62–1.74 (m, 4H), 2.31 (t, J = 7.1 Hz, 2H), 2.71 (t, J = 7.3 Hz, 2H), 2.75 (t, J = 7.4 Hz, 2H), 6.55 ppm (s, 1H); $^{13}C\{^1H\}$ NMR (126 MHz, $CDCl_3$): δ = 13.53, 13.56, 13.86, 21.95, 22.84, 22.97, 25.20, 26.44, 31.13, 32.64, 33.00, 39.67, 124.41, 133.71 ppm; MS (EI): m/z (%): 356 (7) $[M]^+$; elemental analysis calcd (%) for $C_{14}H_{28}Se_2$: C 47.46, H 7.97, Se 44.57; found: C 47.38, H 7.99, Se 44.64.

N-[(2Z)-2,3-Bis(butylselanyl)-2-propenyl]-N,N-dimethylamine (2o): Light yellow oil; 88% (0.313 g); 1H NMR (500 MHz, $CDCl_3$): δ = 0.81 (m, 6H), 1.33 (m, 4H), 1.52–1.64 (m, 4H), 2.12 (s, 6H), 2.63 (t, J = 7.3 Hz, 2H), 2.74 (t, J = 7.3 Hz, 2H), 2.94 (s, 2H), 6.73 ppm (s, 1H); $^{13}C\{^1H\}$ NMR (126 MHz, $CDCl_3$): δ = 13.24, 13.27, 22.46, 22.66, 24.81, 26.15, 32.44, 32.76, 44.68, 67.62, 127.84, 129.48 ppm; MS (EI): m/z (%): 357 (16) $[M]^+$; elemental analysis calcd (%) for $C_{13}H_{27}NSe_2$: C 43.95, H 7.66, N 3.94, Se 44.45; found: C 44.09, H 7.51, N 4.20, Se 44.50.

N-[(2Z)-2,3-Bis(methylselanyl)-2-propenyl]-N,N-dimethylamine (2p): Light yellow oil; 59% (0.159 g); 1H NMR (500 MHz, $CDCl_3$): δ = 2.10 (s, 3H), 2.14 (s, 9H), 2.96 (s, 2H), 6.66 ppm (s, 1H); $^{13}C\{^1H\}$ NMR (126 MHz, $CDCl_3$): δ = 5.02, 6.54, 44.68, 66.66, 126.78, 130.28 ppm; MS (EI): m/z (%): 273 (11) $[M]^+$; elemental analysis calcd (%) for $C_7H_{15}NSe_2$: C 31.01, H 5.58, N 5.17, Se 58.25; found: C 30.83, H 5.65, N 5.28, Se 58.11.

Scaling synthetic procedure: $[Ni(acac)_2]$ (3.0×10^{-4} mol, 77.0 mg), Bu_2Se_2 (1.0×10^{-2} mol, 1.784 g) and PMe_2Ph (3.0×10^{-3} mol, 0.415 g) were placed in a reaction vessel and stirred at room temperature until a homogeneous brown solution was formed (ca. 5–10 min). The alkyne **1a** (1.0×10^{-2} mol, 0.821 g) was added to the solution and the stirring was continued for additional 10 min. The reaction was carried out for 2 h at 100 °C under stirring. Isolated yield after purification on silica: 78% (2.120 g).

Preparation of Bu_2Se_2 :^[36] The synthesis was carried out at 20 °C under argon atmosphere under rigorous stirring. Se powder (4.0 g, 0.05 mol; 200 mesh) was placed into two-necked flask followed by addition of EtOH (80%, 150 mL). $NaBH_4$ (3.8 g, 0.1 mol) was slowly added to the solution (*Caution*: gas evolution at this stage) until complete dissolution of Se and formation of colorless suspension with white-gray solid (a slight excess of $NaBH_4$ might be required). DMF (100 mL) was added to the solution and it was stirred until the color was turned to red-brown (ca. 10 min). EtOH (80%, 50 mL) was added to the solution and stirring was continued until termination of gas evolution (traces of unreacted hydrides should be removed). Se powder (4.0 g, 0.05 mol; 200 mesh) was added to the solution and stirred until complete dissolution and formation of clear dark-red solution. $BuBr$ (13.7 g, 0.1 mol) was slowly added to the solution during 30 min, changing its color to yellow. The reaction was quenched by addition of water (300 mL) and extracted by hexanes (3×200 mL). The combined organic phase was washed with water (3×500 mL) and dried over Na_2SO_4 . The solvent was removed under reduced pressure and pure product was obtained after distillation (55–57 °C, 0.06 Torr), yellow-orange oil, yield 12.33 g (90%).

Theoretical calculations: Geometry and energy of the reactants, intermediates, transition states, and products of the reactions were calculated using the B3LYP hybrid density functional method^[37] in conjunction with the standard 6–311G(d) basis set^[38] for H, C, P, S, and Se and the triple- ζ basis set with the Stuttgart/Dresden effective core potentials^[39] (SDD) for Pd and Ni (denoted as B3LYP/SDD 6–311G(d) level). In previous studies it was established that this level of theory reasonably describes the energy and geometry parameters of the systems involving transition metal complexes.^[40]

For all studied structures, normal coordinate analysis was performed to characterize the nature of the stationary points and to calculate thermodynamic properties (298.15 K and 1 atm). Transition states were confirmed with IRC (intrinsic reaction coordinate) calculations by using the standard method.^[41] All calculations were performed without any symmetry constraints with the Gaussian 03 program.^[42]

Table 15. Crystallographic data for **2i**, **2e**, **2k**, and **2m**.

	2i -HOOC-COOH	2e -HOOC-COOH	2k -HOOC-COOH	2m -HOOC-COOH
formula	C ₉ H ₁₇ NO ₄ S ₂	C ₁₅ H ₂₉ NO ₄ S ₂	C ₁₃ H ₂₅ NO ₄ S ₂	C ₁₉ H ₃₃ NO ₄ S ₂
<i>M</i> _r	267.36	351.51	323.46	403.58
<i>T</i> [K]	100	100	100	100
cryst size [mm]	0.50 × 0.05 × 0.05	0.30 × 0.30 × 0.06	0.30 × 0.30 × 0.20	0.40 × 0.05 × 0.05
crystal system	monoclinic	monoclinic	monoclinic	orthorhombic
space group	<i>C2/c</i>	<i>Pc</i>	<i>P2₁/c</i>	<i>Pca2₁</i>
<i>a</i> [Å]	28.823(6)	8.3017(7)	8.2680(5)	25.195(5)
<i>b</i> [Å]	5.5553(13)	21.9390(18)	20.6710(12)	15.550(3)
<i>c</i> [Å]	16.177(4)	11.0390(9)	11.0938(7)	11.045(2)
<i>α</i> [°]	90	90	90	90
<i>β</i> [°]	92.681(6)	107.725(5)	110.925(5)	90
<i>γ</i> [°]	90	90	90	90
<i>V</i> [Å ³]	2587.5(10)	1915.1(3)	1770.97(19)	4327.2(15)
<i>Z</i>	8	4	4	8
<i>ρ</i> _{calcd} [g cm ⁻³]	1.373	1.219	1.213	1.239
<i>F</i> (000)	1136	760	696	1744
<i>μ</i> [mm ⁻¹]	0.410	0.293	0.311	0.269
<i>θ</i> range [°]	1.41 to 27.99	1.86 to 30.04	1.97 to 30.04	1.62 to 26.14
index range	−37 ≤ <i>h</i> ≤ 37 −7 ≤ <i>k</i> ≤ 7 −21 ≤ <i>l</i> ≤ 21	−11 ≤ <i>h</i> ≤ 11 −30 ≤ <i>k</i> ≤ 30 −15 ≤ <i>l</i> ≤ 15	−11 ≤ <i>h</i> ≤ 11 −29 ≤ <i>k</i> ≤ 29 −15 ≤ <i>l</i> ≤ 15	−31 ≤ <i>h</i> ≤ 31 −19 ≤ <i>k</i> ≤ 18 −13 ≤ <i>l</i> ≤ 13
reflns collected	13 686	23 430	22 765	32 015
unique rflns	3092 (<i>R</i> _{int} = 0.0606)	10 962 (<i>R</i> _{int} = 0.0318)	5123 (<i>R</i> _{int} = 0.0271)	8500 (<i>R</i> _{int} = 0.0707)
reflns with <i>I</i> > 2σ(<i>I</i>)	1492	8624	4477	3831
<i>R</i> 1/ <i>wR</i> 2 [<i>I</i> > 2σ(<i>I</i>)]	0.0569/0.0561	0.0619/0.1432	0.0281/0.0687	0.0772/0.1367
<i>R</i> 1/ <i>wR</i> 2 (all data)	0.1673/0.0723	0.0828/0.1583	0.0346/0.0727	0.2046/0.1756
data/restraints/parameters	3092/0/149	10962/22/369	5123/0/187	8500/26/437
GOF on <i>F</i> ²	0.932	1.002	1.004	1.014
largest diff peak/hole (e [−] Å ^{−3})	0.420/−0.443	0.838/−0.812	0.447/−0.285	0.610/−0.460
max/min transmission	0.979/0.821	0.989/0.919	0.942/0.912	0.989/0.909
absolute structure parameter	−	0.05(7)	−	0.00(12)

X-ray crystal structure determination: Data were collected on a Bruker three-circle diffractometer equipped with a SMART APEX II CCD detector and corrected for absorption using the SADABS program.^[43] Data reduction was performed by using APEX2^[44] and SAINTPlus^[45] programs. For details, see Table 15. The structures were solved by direct methods and refined by full-matrix least-squares techniques on *F*² with anisotropic displacement parameters for all the non-hydrogen atoms. The two butyl groups in **2e** and one cyclohexyl group in **2m** were disordered over two sites each with occupancies of 0.65:0.35, 0.65:0.35, and 0.60:0.40, respectively. The amino-hydrogen atoms of the cations and hydroxy-hydrogen atoms of the anions were localized in the difference Fourier syntheses and included in the refinement with fixed positional and isotropic displacement parameters. The other hydrogen atoms were placed in calculated positions and refined within the riding model with fixed isotropic displacement parameters (*U*_{iso}(H) = 1.5 *U*_{eq}(C) for the CH₃ groups and *U*_{iso}(H) = 1.2 *U*_{eq}(C) for the other groups). All calculations were carried out using the SHELXTL (PC Version 6.12) program.^[46]

CCDC 656216 (**2e**), 656217 (**2i**), 656218 (**2k**), and 656219 (**2m**) contain the supplementary crystallographic data for this paper. These data can be obtained free of charge from The Cambridge Crystallographic Data Centre via www.ccdc.cam.ac.uk/data_request/cif.

Acknowledgements

The research work was supported by the Russian Foundation for Basic Research (Project No. 07-03-00851), Research grant MD-4094.2007.3, and Program No 1 of Division of Chemistry and Material Sciences of RAS. We thank Prof. T. V. Timofeeva for fruitful discussion of X-ray structures and help in this work.

- a) H. Kuniyasu, A. Ogawa, S. Miyazaki, I. Ryu, N. Kambe, N. Sonoda, *J. Am. Chem. Soc.* **1991**, *113*, 9796; b) A. Ogawa, *J. Organomet. Chem.* **2000**, *611*, 463.
- Related reviews on the field: a) *Catalytic Heterofunctionalization* (Eds.: A. Togni, H. Grützmacher) Wiley-VCH, Weinheim, **2001**; b) M. Beller, J. Seayad, A. Tillack, H. Jiao, *Angew. Chem.* **2004**, *116*, 3448; *Angew. Chem. Int. Ed.* **2004**, *43*, 3368; c) T. Kondo, T. Mitsudo, *Chem. Rev.* **2000**, *100*, 3205; d) I. Beletskaya, C. Moberg, *Chem. Rev.* **2006**, *106*, 2320; e) F. Alonso, I. P. Beletskaya, M. Yus, *Chem. Rev.* **2004**, *104*, 3079.
- I. P. Beletskaya, V. P. Ananikov, *Eur. J. Org. Chem.* **2007**, 3431.
- a) V. P. Ananikov, I. P. Beletskaya, G. G. Aleksandrov, I. L. Eremenko, *Organometallics* **2003**, *22*, 1414; b) V. P. Ananikov, M. A. Kabeshov, I. P. Beletskaya, G. G. Aleksandrov, I. L. Eremenko, *J. Organomet. Chem.* **2003**, *687*, 451; c) V. P. Ananikov, M. A. Kabeshov, I. P. Beletskaya, V. N. Khrustalev, M. Yu. Antipin, *Organometallics* **2005**, *24*, 1275; d) V. P. Ananikov, I. P. Beletskaya, *Org. Biomol. Chem.* **2004**, *2*, 284; e) V. P. Ananikov, M. A. Kabeshov, I. P. Beletskaya, *Synlett* **2005**, 1015.
- a) M. Arisawa, M. Yamaguchi, *Org. Lett.* **2001**, *3*, 763; b) M. Arisawa, Y. Kozuki, M. Yamaguchi, *J. Org. Chem.* **2003**, *68*, 8964.
- a) H. Kuniyasu, A. Ogawa, K. Sato, I. Ryu, N. Kambe, N. Sonoda, *J. Am. Chem. Soc.* **1992**, *114*, 5902; b) H. Kuniyasu, A. Ogawa, K.-I. Sato, I. Ryu, N. Sonoda, *Tetrahedron Lett.* **1992**, *33*, 5525; c) I. Kamiya, E. Nishinaka, A. Ogawa, *J. Org. Chem.* **2005**, *70*, 696.
- a) C. Cao, L. R. Fraser, J. A. Love, *J. Am. Chem. Soc.* **2005**, *127*, 17614; b) V. Circu, M. A. Fernandes, L. Carlton, *Polyhedron* **2003**, *22*, 3293; c) Y. Misumi, H. Seino, Y. Mizobe, *J. Organomet. Chem.* **2006**, *691*, 3157.
- a) V. P. Ananikov, N. V. Orlov, I. P. Beletskaya, *Organometallics* **2006**, *25*, 1970; b) V. P. Ananikov, N. V. Orlov, I. P. Beletskaya, *Organometallics* **2007**, *26*, 740; c) V. P. Ananikov, D. A. Malyshev, I. P.

- Beletskaya, G. G. Aleksandrov, I. L. Eremenko, *Adv. Synth. Catal.* **2005**, *347*, 1993.
- [9] V. P. Ananikov, N. V. Orlov, I. P. Beletskaya, V. N. Khrustalev, M. Yu. Antipin, T. V. Timofeeva, *J. Am. Chem. Soc.* **2007**, *129*, 7252.
- [10] *Organoselenium Chemistry: Modern Developments in Organic Synthesis* (Ed.: T. Wirth), Springer, Berlin, **2000**.
- [11] Some representative examples: a) S. D. P. Baugh, Z. Yang, D. K. Leung, D. M. Wilson, R. Breslow, *J. Am. Chem. Soc.* **2001**, *123*, 12488; b) B. J. Vesper, K. Salaita, H. Zong, C. A. Mirkin, A. G. M. Barrett, B. M. Hoffman, *J. Am. Chem. Soc.* **2004**, *126*, 16653; c) S. Belviso, G. Ricciardi, F. Lelj, *J. Mater. Chem.* **2000**, *10*, 297; d) S. H. Eichhorn, D. W. Bruce, D. Guillon, J.-L. Gallani, T. Fischer, J. Stumpe, T. Geue, *J. Mater. Chem.* **2001**, *11*, 1576; e) F. Bonosi, G. Ricciardi, F. Lelj, G. Martini, *J. Phys. Chem.* **1994**, *98*, 10613; f) S. B. Sesalan, A. Gul, *Monatsh. Chem.* **2000**, *131*, 1191; g) H. Braun, A. Amann, *Angew. Chem.* **1975**, *87*, 773; *Angew. Chem. Int. Ed. Engl.* **1975**, *14*, 755; h) M. E. Garst, P. Arrhenius, *J. Org. Chem.* **1983**, *48*, 16.
- [12] a) S. W. Benson, *Chem. Rev.* **1978**, *78*, 23; b) S. Antonello, R. Benassi, G. Gavioli, F. Taddei, F. Maran, *J. Am. Chem. Soc.* **2002**, *124*, 7529.
- [13] Internal alkynes were inactive in the catalytic reaction as was found for the 4-octyne and bis(trimethylsilyl)acetylene.
- [14] Competitive noncatalytic side-reaction of E–E bond addition to alkynes (path b; Scheme 1) decreased the overall selectivity in the case of diaryldisulfides (see ref. [3]). This noncatalytic reaction was not observed in dialkyldisulfides addition to alkynes under studied conditions.
- [15] We were unable to carry out the catalytic reaction of **1a** with *t*Bu₂S₂ and diadamantylidysulfide. This finding confirms the influence of bulky substituents bonded to the sulfur atom on the reactivity of dialkyldisulfides.
- [16] a) D. S. Pedersen, C. Rosenbohm, *Synthesis* **2001**, 2431; b) L. M. Harwood, *Aldrichimica Acta* **1985**, *18*, 25.
- [17] Dry column flash chromatography has several practical advantages: 1) small amount of silica required; 2) quick elution; 3) economy of solvents. However, slightly better isolated yields (by \approx 5–10%) may be achieved using conventional column chromatography.
- [18] Using higher temperatures and shorter reaction time is also possible. However, it requires special attention to experimental equipment (high pressure may develop in reaction vessel) and in some cases may facilitate side reactions.
- [19] See also published X-ray structure in reference [4b].
- [20] See also published X-ray structures in references [8c,9].
- [21] a) G. Mughesh, H. B. Singh, *Chem. Soc. Rev.* **2000**, *29*, 347; b) G. Mughesh, W.-W. du Mont, H. Sies, *Chem. Rev.* **2001**, *101*, 2125.
- [22] a) C. Bleiholder, R. Gleiter, D. B. Werz, H. Koppel, *Inorg. Chem.* **2007**, *46*, 2249; b) M. Tiecco, L. Testaferri, C. Santi, C. Tomassini, S. Santoro, F. Marini, L. Bagnoli, A. Temperini, F. Costantino, *Eur. J. Org. Chem.* **2006**, 4867; c) M. Iwaoka, S. Takemoto, M. Okada, S. Tomoda, *Bull. Chem. Soc. Jpn.* **2002**, *75*, 1611; d) M. Iwaoka, S. Takemoto, M. Okada, S. Tomoda, *Chem. Lett.* **2001**, *30*, 132; e) D. Pal, P. Chakrabarti, *J. Biomol. Struct. Dyn.* **2001**, *19*, 115; f) R. M. Minyaev, V. I. Minkin, *Can. J. Chem.* **1998**, *76*, 776.
- [23] For clarity reasons only mononuclear metal species are shown on Scheme 4 to illustrate the nature of the elementary steps of the catalytic cycle.
- [24] It is a known fact that Ni compounds very often result in broad NMR signals of unacceptable quality, see: *Transition Metal Nuclear Magnetic Resonance* (Ed.: P. S. Pregosin), Elsevier, Amsterdam, **1991**.
- [25] a) J. M. Gonzales, D. G. Musaev, K. Morokuma, *Organometallics* **2005**, *24*, 4908; b) V. P. Ananikov, N. V. Orlov, I. P. Beletskaya, *Russ. Chem. Bull.* **2005**, *54*, 576.
- [26] The discussion for the ΔH surface is also valid for the ΔE surface and will not be repeated in the article.
- [27] Since **II** is higher in energy on the ΔG surface than **I** the overall **1**→**III-TS** barrier should be taken into account.
- [28] It was not possible to locate the corresponding transition state neither by creating several starting geometries by hands nor by QST (STQN) method built in Gaussian 03 package. In all cases the structures were converged to the product **IV** during geometry optimization. Most likely, this indicates that the actual activation barrier is rather small and it was impossible to locate due to exothermic reaction. To ensure that this is not a failure of B3LYP, the calculations for this transition state were repeated at MP2 level and led to the same result.
- [29] Preliminary estimation based on the calculations of the oxidative addition step. The actual mechanism of C–E bond breakage could be quite complicated, see for example the study involving diaryldichalcogenides (ref. [25b]).
- [30] a) H. Kuniyasu, F. Yamashita, J. Terao, N. Kambe, *Angew. Chem.* **2007**, *119*, 6033; *Angew. Chem. Int. Ed.* **2007**, *46*, 5929; b) T. Sagawa, Y. Sakamoto, R. Tanaka, H. Katayama, F. Ozawa, *Organometallics* **2003**, *22*, 4433; c) K. Sugoh, H. Kuniyasu, H. Kurosawa, *Chem. Lett.* **2002**, 106.
- [31] a) I. P. Beletskaya, V. P. Ananikov, *Pure Appl. Chem.* **2007**, *79*, 1041; b) Q. Cui, D. G. Musaev, K. Morokuma, *Organometallics* **1997**, *16*, 1355; c) Q. Cui, D. G. Musaev, K. Morokuma, *Organometallics* **1998**, *17*, 742.
- [32] a) P. W. Jolly, G. Wilke, *The Organic Chemistry of Nickel*, Academic Press, New York, **1974**; b) “Polymerization of Acetylenes”: T. Masuda, F. Sanda, M. Shiotsuki in *Comprehensive Organometallic Chemistry III, Vol. 11* (Eds.: D. M. P. Mingos, R. H. Crabtree), Elsevier, Oxford, **2007**, pp. 557–593.
- [33] T. Ukai, H. Kawazura, Y. Ishii, J. J. Bonnet, J. A. Ibers, *J. Organomet. Chem.* **1974**, *65*, 253.
- [34] V. P. Ananikov, I. P. Beletskaya, *Russ. Chem. Bull.* **2003**, *52*, 811.
- [35] NMR monitoring (or GC) is the easiest way to determine appropriate reaction time.
- [36] Original synthetic procedure: a) A. Krief, M. Derock, *Synlett* **2005**, 1012; b) A. Krief, M. Trabelsi, W. Dumont, M. Derock, *Synlett* **2004**, 1751.
- [37] a) A. D. Becke, *Phys. Rev. A* **1988**, *38*, 3098; b) C. Lee, W. Yang, R. G. Parr, *Phys. Rev. B* **1988**, *37*, 785; c) A. D. Becke, *J. Chem. Phys.* **1993**, *98*, 5648.
- [38] a) R. Krishnan, J. S. Binkley, R. Seeger, J. A. Pople, *J. Chem. Phys.* **1980**, *72*, 650; b) A. D. McLean, G. S. Chandler, *J. Chem. Phys.* **1980**, *72*, 5639.
- [39] a) P. Schwerdtfeger, M. Dolg, W. H. E. Schwarz, G. A. Bowmaker, P. D. W. Boyd, *J. Chem. Phys.* **1989**, *91*, 1762; b) D. Andrae, U. Häußermann, M. Dolg, H. Stoll, H. Preuß, *Theor. Chim. Acta* **1990**, *77*, 123; c) A. Bergner, M. Dolg, W. Küchle, H. Stoll, H. Preuß, *Mol. Phys.* **1993**, *80*, 1431.
- [40] a) V. P. Ananikov, D. G. Musaev, K. Morokuma, *Organometallics* **2005**, *24*, 715; b) V. P. Ananikov, D. G. Musaev, K. Morokuma, *J. Am. Chem. Soc.* **2002**, *124*, 2839; c) V. P. Ananikov, D. G. Musaev, K. Morokuma, *Organometallics* **2001**, *20*, 1652.
- [41] a) C. Gonzalez, H. B. Schlegel, *J. Chem. Phys.* **1989**, *90*, 2154; b) C. Gonzalez, H. B. Schlegel, *J. Phys. Chem.* **1990**, *94*, 5523.
- [42] Gaussian 03 (Revision C2), M. J. Frisch, G. W. Trucks, H. B. Schlegel, G. E. Scuseria, M. A. Robb, J. R. Cheeseman, J. A. Montgomery Jr., T. Vreven, K. N. Kudin, J. C. Burant, J. M. Millam, S. S. Iyengar, J. Tomasi, V. Barone, B. Mennucci, M. Cossi, G. Scalmani, N. Rega, G. A. Petersson, H. Nakatsuji, M. Hada, M. Ehara, K. Toyota, R. Fukuda, J. Hasegawa, M. Ishida, T. Nakajima, Y. Honda, O. Kitao, H. Nakai, M. Klene, X. Li, J. E. Knox, H. P. Hratchian, J. B. Cross, C. Adamo, J. Jaramillo, R. Gomperts, R. E. Stratmann, O. Yazyev, A. J. Austin, R. Cammi, C. Pomelli, J. W. Ochterski, P. Y. Ayala, K. Morokuma, G. A. Voth, P. Salvador, J. J. Dannenberg, V. G. Zakrzewski, S. Dapprich, A. D. Daniels, M. C. Strain, O. Farkas, D. K. Malick, A. D. Rabuck, K. Raghavachari, J. B. Foresman, J. V. Ortiz, Q. Cui, A. G. Baboul, S. Clifford, J. Cioslowski, B. B. Stefanov, G. Liu, A. Liashenko, P. Piskorz, I. Komaromi, R. L. Martin, D. J. Fox, T. Keith, M. A. Al-Laham, C. Y. Peng, A. Nanayakkara, M. Challacombe, P. M. W. Gill, B. Johnson, W. Chen,

- M. W. Wong, C. Gonzalez, J. A. Pople, Gaussian, Inc., Pittsburgh, PA, **2004**.
- [43] G. M. Sheldrick, SADABS, v. 2.03, Bruker/Siemens Area Detector Absorption Correction Program, Bruker AXS, Madison, Wisconsin (USA), **2003**.
- [44] Bruker AXS, APEX2 software package, Bruker Molecular Analysis Research Tool, v. 1.27, Bruker AXS, Madison, Wisconsin (USA), **2005**.
- [45] Bruker AXS, SAINTPlus for NT, v. 6.2, Data Reduction and Correction Program, Bruker AXS, Madison, Wisconsin (USA), **2001**.
- [46] G. M. Sheldrick, SHELXTL for NT, v. 6.12, Structure Determination Software Suite, Bruker AXS, Madison, Wisconsin (USA), **2001**.

Received: August 17, 2007
Published online: January 21, 2008